On the Function of the 14 Å Long Internal Cavity of Histone Deacetylase-Like Protein: Implications for the Design of Histone Deacetylase Inhibitors

Di-Fei Wang,[†] Olaf Wiest,*[,†] Paul Helquist,[†] Hsuan-Yin Lan-Hargest,[‡] and Norbert L. Wiech[‡]

Department of Chemistry and Biochemistry, University of Notre Dame, Notre Dame, Indiana 46556, and Beacon Laboratories, Phoenix, Maryland 21131

Received February 20, 2004

Histone deacetylases (HDACs) play an important role in gene transcription. Inhibitors of HDACs induce cell differentiation and suppress cell proliferation in tumor cells. AutoDock calculations of known and novel HDAC inhibitors as well as of several probe molecules to histone deacetylase-like protein (HDLP), using a modified scoring function for metalloproteins, demonstrate excellent agreement ($R = 0.92$) between experimental and computed binding constants. Analysis of the docked structures allows a determination of the different binding motifs in known inhibitors. Such calculations are a useful tool for the prediction of binding constants for new HDAC inhibitors. Exploration of the 14 Å long internal cavity adjacent to the active site by docking of small molecular probes suggest that it plays a crucial role by accepting the cleaved acetate and releasing it at the far side of the cavity. The importance of the findings for the design of new inhibitors is discussed.

Introduction

Acetylation and deacetylation of the ϵ-amino group of specific lysines within histones play a crucial role in the transcriptional process.[1] Two families of enzymes, acetylases and deacetylases, are involved in controlling the acetylation state of histones. Recent studies show that inhibition of histone deacetylases (HDACs) elicits anticancer effects in several tumor cells by inhibition of cell growth and induction of cell differentiation. As a result of these findings, several programs for the development of HDAC inhibitors as anticancer drugs have been initiated. Compounds such as the hydroxamic acids trichostatin A (TSA)[2] and suberanilohydroxamic acid (SAHA)[3] or the cyclic tetrapeptides apicidin[4] and trapoxin[5] as well as synthetic inhibitors,[6,28] including our simplified TSA analogue CG1521,[7] have been studied for this purpose in cancer cell lines and in tumor animal models (Chart 1).[8] With no doubt, the inhibition of HDACs is a rapidly growing and very promising area for cancer chemotherapy.[9]

The X-ray crystal structures of an HDAC homologue, histone deacetylase-like protein (HDLP), from *Aquifex aeolicus*, and its TSA and SAHA complexes have been elucidated with 2.0 Å resolution.[10] The X-ray structure revealed that HDLP has a tubelike, 11 Å deep channel (called the channel afterward) which leads to the active site and which accommodates TSA or SAHA (Figure 1). A catalytic zinc ion is at the bottom of this channel. The aliphatic chain of TSA or SAHA has multiple favorable contacts with hydrophobic residues in the channel. Interestingly, there is a 14 Å long internal cavity (called the internal cavity afterward) adjacent to the Zn binding site. A sequence alignment shows a 35.2% sequence identity of HDLP and human HDAC1 (see Figure 11 in Supporting Information). The residues around the HDLP Zn binding site are completely conserved in human HDAC1. All of the hydrophobic residues that make up the 11 Å channel in HDLP are identical in HDAC1. Most of the residues making up the 14 Å internal cavity are either identical or conservatively substituted in HDAC1. As can be expected from the high degree of sequence similarity shown in Figure 11, HDAC has the same structural features of HDLP described above. Since there is no X-ray structure of human HDAC1 available now, we developed a homology model of human HDAC1 based on the HDLP X-ray structure.[11] In particular, both have a tubelike channel adjacent to a long internal cavity (Figure 12 in Supporting Information). Arg27 lies in the internal cavity in both cases. This high degree of similarity suggests that the internal cavity plays a significant role in the reaction that could potentially be exploited for drug development. Similar features can also be found in other class I histone deacetylases.[12]

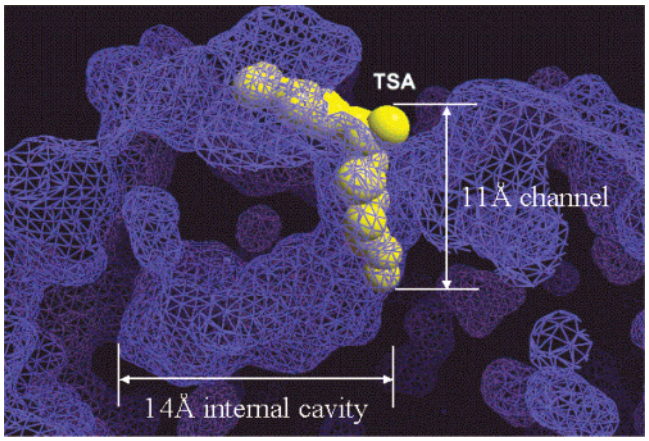

Figure 1. Surface representation of 11 Å channel and 14 Å internal cavity of HDLP. TSA is displayed as a yellow space-filling model.[8]

* To whom correspondence should be sent. Phone: (574) 631 5876. Fax: (574) 631 6652. E-mail: Olaf.G.Wiest.1@nd.edu.
[†] University of Notre Dame.
[‡] Beacon Laboratories.

10.1021/jm0498497 CCC: $27.50
Published on Web 05/25/2004

Chart 1. Known HDAC1 Inhibitors and Novel CG1521 Inhibitor

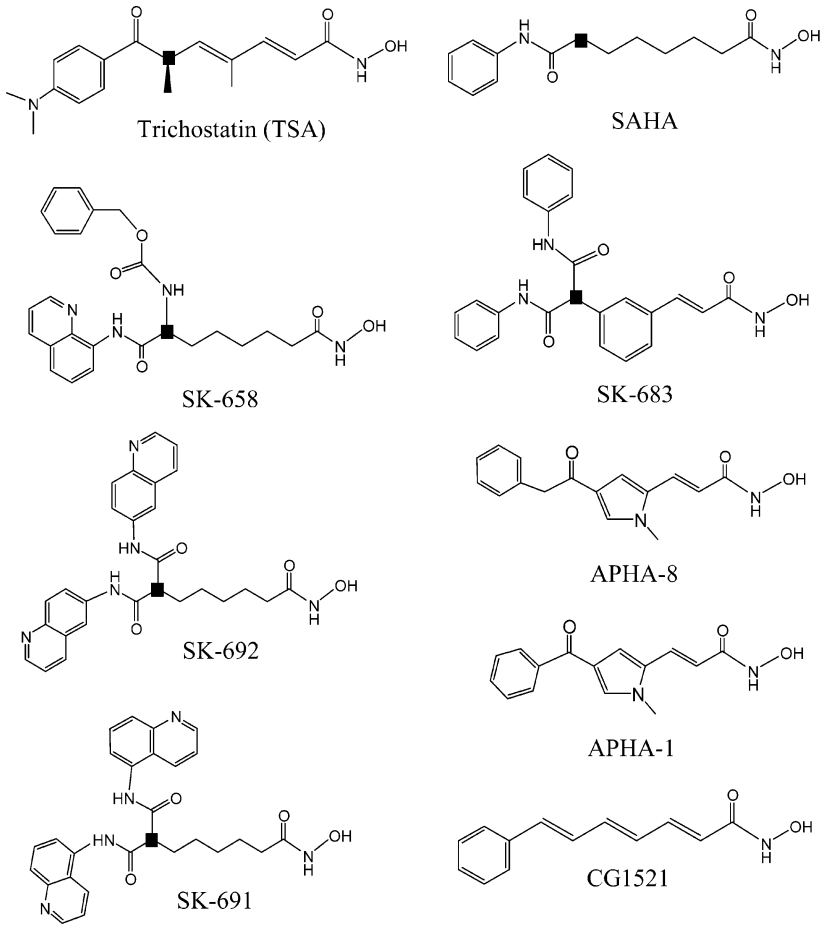

The X-ray structure of the potent HDAC inhibitor TSA bound to HDLP establishes that the function of the channel is to accommodate the acetylated lysine side chain. From this finding it is clear that one of the design strategies for HDAC inhibitors is to utilize this channel to accommodate mimics of the acetylated lysine side chain and its complexation to the essential zinc ion in the active site.[10] The function of the 14 Å long internal cavity, according to the authors of the structural study, "is not clear".[10] One reasonable hypothesis is that it could accommodate the acetate product after the hydrolysis reaction, releasing this byproduct in a separate step. However, no evidence supports this possibility so far.

As part of our effort to develop new histone deacetylase inhibitors, we investigated the binding modes of HDAC inhibitors as well as probe molecules using AutoDock. Here we present the results of validation studies and the docking of the novel HDAC inhibitor CG1521 into the active site of HDLP, indicating that an appropriately modified AutoDock scoring function is able to accurately reproduce the interactions in the active site, the 11 Å channel, and the surface interactions. We also report computational evidence for the possible role of the internal cavity of HDLP/HDAC as a transport vehicle for the acetate byproduct of the hydrolysis reaction. These results provide new concepts for the design of novel HDAC inhibitors.

Computational Methodology. AutoDock 3.0[13] was used for all docking calculations. Through precalculated grids of affinity potentials, it evaluates suitable ligand positions on a given protein. It allows random movements of multiple ligand conformations of the ligand on the protein surface while the protein is required to be rigid. Therefore, it is possible to explore the potential binding pocket or binding modes for studying protein−ligand interaction. A free energy scoring function in the AutoDock3.0 program,[13] which is based on a linear regression analysis, the AMBER force field, and a large set of diverse protein−ligand complexes with known inhibition constants were used to investigate the different ligand binding affinities. Several detailed studies by the McCammon group on binding modes and affinity of HIV-1 integrase inhibitors have shown that the estimated free energies from the AutoDock program are in good agreement with the available experimental values.[14] The AutoDockTools[15] package was employed to generate the docking input files and to analyze the docking results. A grid box size of $90 \times 90 \times 90$ with a spacing of 0.375 Å between the grid points was implemented and covered almost the entire HDLP surface. For TSA, SAHA, CG1521, and other inhibitors, the single bonds except the amide bonds were treated as active torsional bonds (see all structures in Chart 1). One hundred docked structures, i.e. 100 runs, were generated by using genetic algorithm searches. A default protocol was applied, with an initial population of 50 randomly placed individuals, a maximum number of 2.5×10^5 energy evaluations, and a maximum number of 2.7×10^4 generations. A mutation rate of 0.02

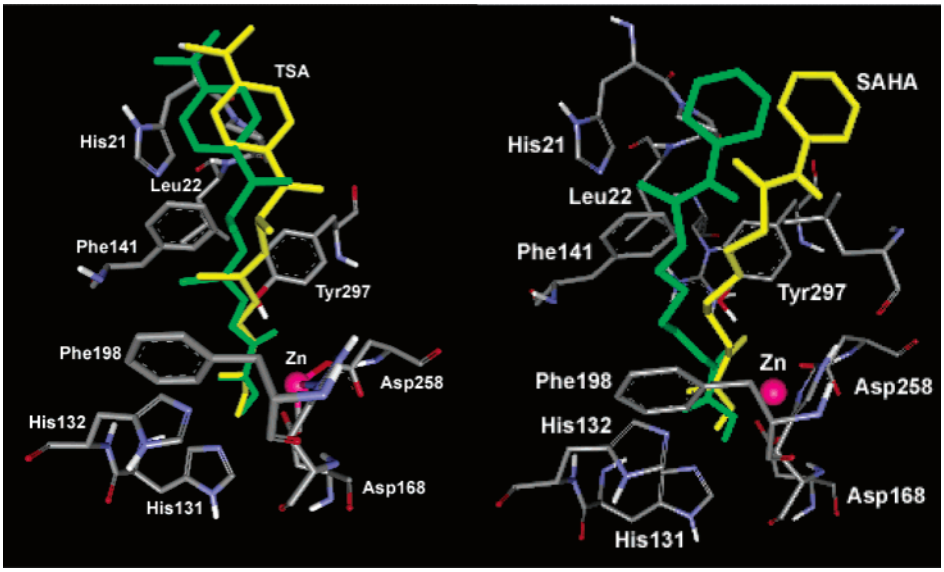

Figure 2. Comparison of X-ray structure (yellow) and the best docked structures (green) of the HDLP−TSA complex (left) and HDLP−SAHA (right).

and a crossover rate of 0.8 were used. Results differing by less than 0.5 Å in positional root-mean-square deviation (RMSD) were clustered together and represented by the result with the most favorable free energy of binding. The RMSD values reported in this work are based upon all heavy atom comparisons between the docked structures and the initial structures.

The structure of HDLP with TSA, PDB code 1c3r,[16] was taken directly from the Protein Data Bank.[17] The xleap module in Amber 6.0 package[18] was used to generate the missing hydrogens in this structure. The united partial charges for protein atoms were taken from the Amber force field. The partial charges for all docked ligands were derived from two-step electrostatic potential (ESP) calculations in the Amber 6.0 package after HF/6-31G* or HF/6-31+G* (if the species is in anionic form) single point calculations by using the Gaussian package.[19] These ligand partial charges were further modified by using the AutoDockTools package so that the charges of the nonpolar hydrogen atoms were assigned to the atom to which the hydrogen is attached.

Although there are many successful examples of structures of protein−ligand,[20] protein−protein,[21] and protein-oligosugar[22] systems studied by the AutoDock program, there are only a few examples of docking studies of metalloprotein−ligand systems in the literature.[23] This paucity is due to the difficulty in finding the proper force field parameters for metal centers in metalloproteins. Since for the purpose of flexible docking calculations a nonbonded model for a metal center is more realistic than a bonded one, we used the nonbonded Zn parameters of Stote et al.[24] which were used successfully in several molecular dynamics studies.[25] Nevertheless, these parameters have to the best of our knowledge not yet been used in docking calculations and need to be validated.

Results and Discussion

Parameters and Docking Validation. The rapid evaluation of binding constants for HDAC would be a highly desirable tool for discovering new HDAC inhibitors. Although different docking programs are available, no energy function is available for metalloproteins such as HDAC. This prompted, for example, the recent development of a QM/MM scoring function for the binding studies of inhibitors of carbonic anhydrase and carboxypeptidase.[26] However, the use of an appropriately modified empirical scoring function is significantly less demanding on computational resources and thus allows the rapid evaluation of a large number of binders. We started our docking study by validating the Zn parameters for use in AutoDock calculations. There are two X-ray structures of HDLP−TSA (PDB code, 1c3r) and HDLP−SAHA (PDB code, 1c3s) complexes available so far, which can be used for method performance evaluation. To be consistent in the subsequent docking studies of other compounds, only the protein structure in 1c3r was used because it (2.0 Å) has a better resolution than 1c3s (2.5 Å). Figure 2 shows the comparison of the docking structures of HDLP−TSA, HDLP−SAHA and their initial structures. Numerical results are summarized in Table 1. Of 100 genetic algorithm runs, the best docked structure of TSA (green) has a RMSD of 0.9 Å compared to its corresponding X-ray structure (yellow) in Figure 2, left. In comparison with the X-ray structure of TSA in the channel, the

Table 1. Calculated and Experimental $\Delta G_{binding}$ (in kcal/mol)

	ΔG_{cal}	ΔG_{exp}	N^a	RMSD (Å)^c
TSA	−9.7	−10.3[7]	2	0.90
SAHA	−7.6	−8.6[7]	6	1.94
SK-658	−11.0	−11.7[27]	1	23.66
SK-683	−12.8	−12.3[27]	1	3.04
SK-692	−11.9	−12.3[27]	1	4.13
APHA-8	−9.4	−8.6[28a]	2	1.71
CG1521[b]	−8.6	−7.8[7]	1	9.06
	−8.3		1	2.43
AcNHOH	−5.6	NA[d]	8	0.59
AcO-	−5.3	NA[d]	3	1.54
HOAc	−4.0	−3.2	2	1.75

[a] N is the number of structures in the first cluster except CG1521. For CG1521, N is the number of structures in the first and second clusters. [b] Two different binding modes were found. See discussion. [c] Initial structures were manually put near the active site except TSA. For TSA, it is the original X-ray structure. All RMSD values here are from all atom-based superimposition against the initial structure. [d] Not available.

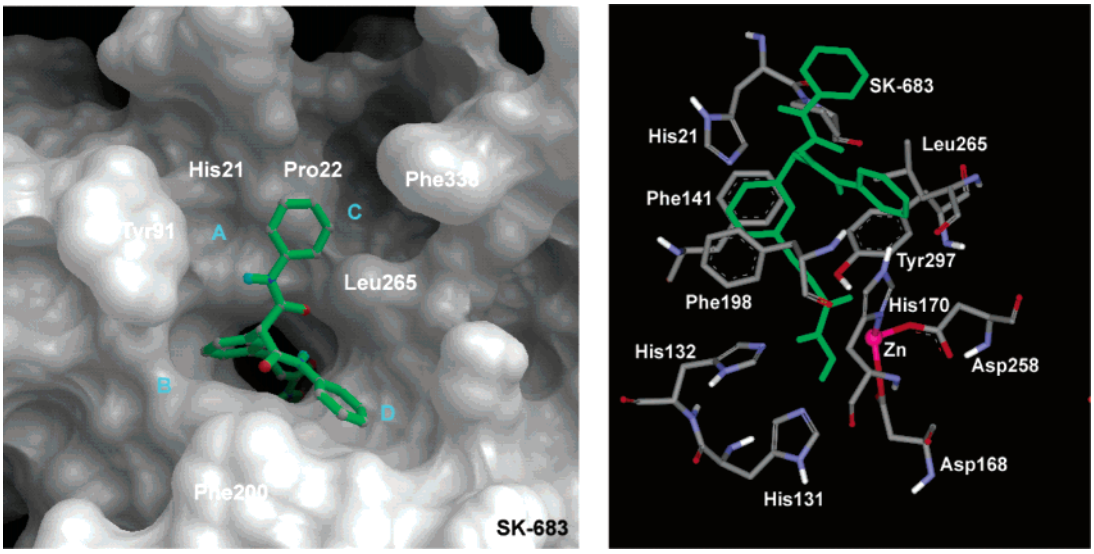

Figure 3. View of surface and active site of SK-683 bound to HDLP.

docked structure has similar multiple interactions with the residues, His131, His132, Tyr297, Phe141, Phe198, etc. For the Zn binding part of TSA, the calculation also gave a reasonable geometry. The distances of Zn···O(C) and Zn···O(H) are 2.45 and 2.24 Å in the X-ray structure while they are 2.54 and1.84 Å in the best docked structure. The following three binding clusters have very similar structures. The RMSDs are 1.1, 1.2, and 3.3 Å compared to the X-ray structure, respectively. The structure with RMSD 3.3 Å shows that the aromatic end group interacts with a very shallow pocket containing His170, Gln192, Tyr196, Ala197, and Leu265. Interestingly, the results in a 2001 patent show that the additional aromatic group attached at the kink carbon position in TSA significantly enhances the HDAC inhibition activity.[27] The origin and potential applications of this finding will be discussed later.

The quality of the docking results is very similar for the second test system, the HDLP−SAHA complex, shown on the right in Figure 2. In these calculations, the protein coordinates of the TSA complex 1c3r were used. The long chain of SAHA fits into the channel quite well. The aliphatic chain is positioned between the two phenyl groups, forming the favorable C−H···π interactions in analogy to the methyl group close to the hydroxamic acid tail in TSA. The results from these two test cases indicate that AutoDock, combined with the nonbonded Zn-parameters provided by Stote and Karplus,[24] is suitable for studying HDLP−ligand interactions. It should also be pointed out that in a recent study, Mai and co-workers manually mutated the related residues within 12 Å around the 11 Å channel of HDLP to those of HDAC1.[28a] By using this small HDAC1 model, three different docking programs, AutoDock, Dock, and GRAMM, were tested and were consistent with our results. AutoDock was found to reproduce the experimental results best.[28a]

Docking of SK-658, SK-683, SK-692, APHA-8, and CG1521. Recently, SK-658, SK-683, and SK-692 with IC_{50} values of 2.5, 1, and 1 nM have been reported as new, strong inhibitors of HDAC1.[27] To understand how these HDAC1 inhibitors bind to the protein, docking studies were performed following the same procedure described above. The results for SK-683 are shown in Figure 3. Molecular surface visualization showed that there are four shallow pockets (A, B, C, and D) on the HDLP surface, Figure 3. Interactions of these pockets with the aromatic groups could enhance the binding ability. In analogy to the structures described above, the cinnamyl chain fits into the 11 Å channel, the NHOH group binds to the Zn ion, and there are hydrogen bond interaction with His131 and His132. For example, SAHA has one terminal aromatic group accommodated in pocket B and has an IC_{50} of 200 nM. When the additional aromatic group of SK-658 was introduced at the kink atom in SAHA using an amide bond linkage, Chart 1, it greatly decreased the IC_{50} to 1 nM. These shallow pockets may be present in human HDAC1 as the sequence of this region is highly conserved compared to HDLP. The docking study of SK-692 shows that the linear fused polyaromatic rings fit quite well in the narrow pocket. Thus, SK-691, an isomer of SK-692, has 100-fold less inhibition activity than SK-692 owing to fewer favorable interactions with these pockets. SK-658 has a binding mode very similar to SK-692. It is worth mentioning that SK-683 is a TSA-like HDAC1 inhibitor. The linker containing a meta-substituted benzene ring moiety is a good mimic of the linker in TSA. Like the behavior of the methyl group close to the NHOH site in TSA, this benzene ring is stacked between the two parallel phenyl rings of residues Phe141 and Phe198, which exist in both HDLP and HDAC1 and form favorable $\pi-\pi$ interactions. The two aromatic side chains are pointing to pockets B and D, as shown in Figures 13 and 14 in the Supporting Information.

APHAs, 3-(4-aroyl-1*H*-2-pyrrolyl)-*N*-hydroxy-2-propenamides, are a novel series of HDAC inhibitors which have been recently studied by Mai and co-workers.[28] Among structures presented there, APHA-8 is the most active one to inhibit maize histone deacetylase (HD2) and mouse histone deacetylase 1 (mHDAC1). It has pIC50 values of 6.29 and 7.00 for mHDAC1 and HD2, respectively. Interestingly, it was found that APHA-1, which has a structure very similar to APHA-8, has a different binding pattern in the active site.[6e,28a] For APHA-8, the pyrrole-ethylene chain interacts with the Phe 141 and Phe 198 residues; the pyrrole-N_1-methyl group has favorable interactions with the α-carbon atom

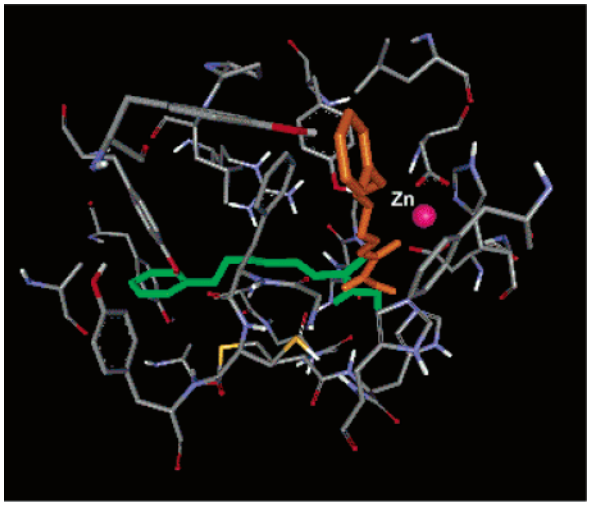

Figure 4. Two calculated binding modes of CG1521 in the 11 Å channel (orange) and in the 14 Å cavity (green).

of Gly140 and partially with the Phe141 side chain. When we docked APHA-8 into the active site of HDLP, we found the pyrrole-ethylene chain of APHA-8 has a binding pattern similar to the one postulated by Mai et al.[28a] However, the N_1-methyl group is similar to the C4-methyl group in TSA, intercalated by the two parallel Phe 141 and 198 residues and forms favorable CH$\cdots\pi$ interactions. The pyrrole C4-phenylacetyl portion occupies pocket D on the surface (see Figure 15 in the Supporting Information). The distances of Zn$\cdots$OH(NHC=O) and Zn$\cdots$O=C(NHOH) are 2.71 and 1.97 Å, respectively. They are slightly shorter than these in the HDLP−TSA complex (Zn$\cdots$OH(NHC=O), 2.24 Å and Zn$\cdots$O=C(NHOH), 2.45 Å).

These results encouraged us to study CG1521, which is structurally similar to TSA and which also has shown remarkable antiproliferative activity in the PC-3 cell line and good HDAC1 inhibition activity in the nanomolar range.[7] No X-ray structure of the HDLP−CG1521 complex is available so far. Following the above studies of TSA, SAHA, and SK compounds, we docked CG1521 into the active site of HDLP. Two different types of binding modes of CG1521 to HDLP have been found. One is close to the normal binding mode of TSA in the 11 Å channel. In comparison with the input structure, it has an RMSD of 2.4 Å (see the orange structure in Figure 4). The estimated free energy of binding of −8.3 kcal/mol for this structure is close to the experimental value of −7.8 kcal/mol.

More interestingly, we also found a second binding mode, where CG1521 is lying in the 14 Å internal cavity with a free energy of binding of −8.6 kcal/mol, as shown by the green structure in Figure 4. While the hydroxamic acid group coordinates the Zn ion, the phenyl group tail is directed deeply into the internal cavity. Although it is unlikely that the channel around the active site would allow this binding mode, this result does suggest that the cavity could be exploited to gain additional binding sites in the design of new types of HDAC inhibitors. This concept will be discussed in more detail below.

A second design element that emerges from these studies is possible interactions with the hydrophobic pockets on the surface of HDLP near the exit of the channel. TSA interacts with only one of these pockets. The understanding that can be derived from HDLP−ligand docking study can be used to design stronger and more specifically binding ligands for HDLP or HDAC1. From the results discussed above, a new class of structure with three branched aromatic groups can be proposed. The docked structure of one such inhibitor is shown in Figure 5. It can be seen that the new ligands of this type interact strongly with three of the hydrophobic pockets on the HDLP surface, providing selective binding interactions in addition to the interactions in the channel. Furthermore, the benzyl groups could be functionalized in para position to modulate other properties such as solubility. The synthesis and biological assays of this class of compounds gave indeed very promising results and will be reported separately.[29]

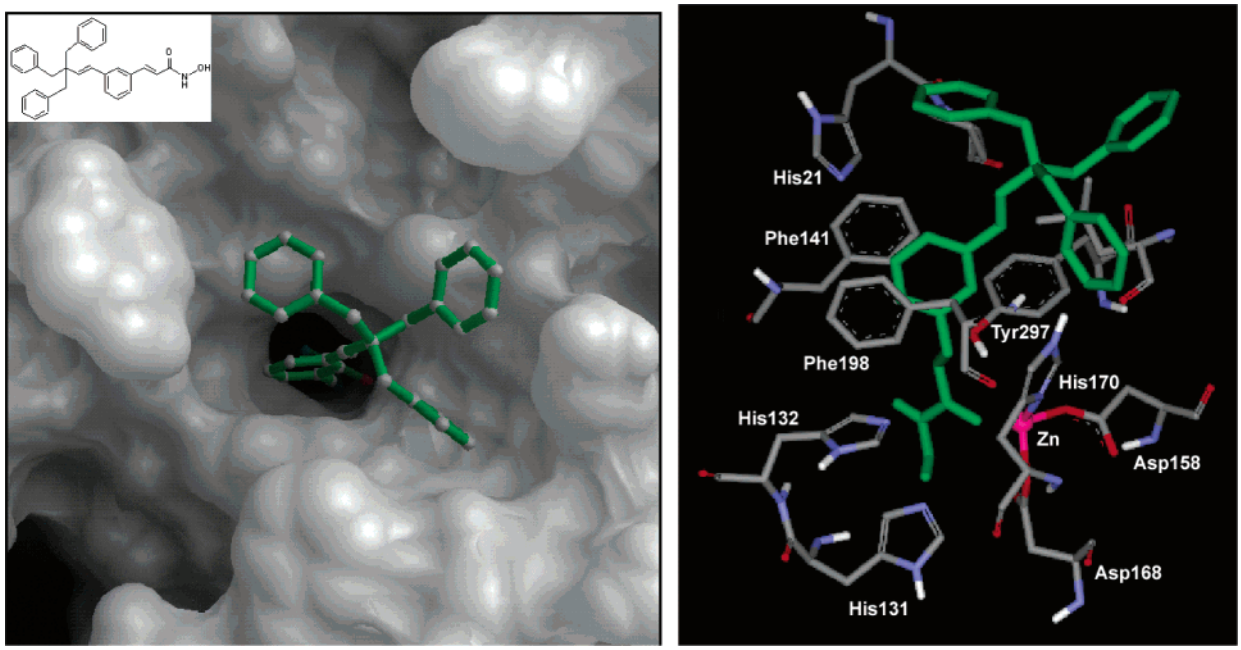

Figure 5. New proposed inhibitor with multiple interactions with the HDLP surface.

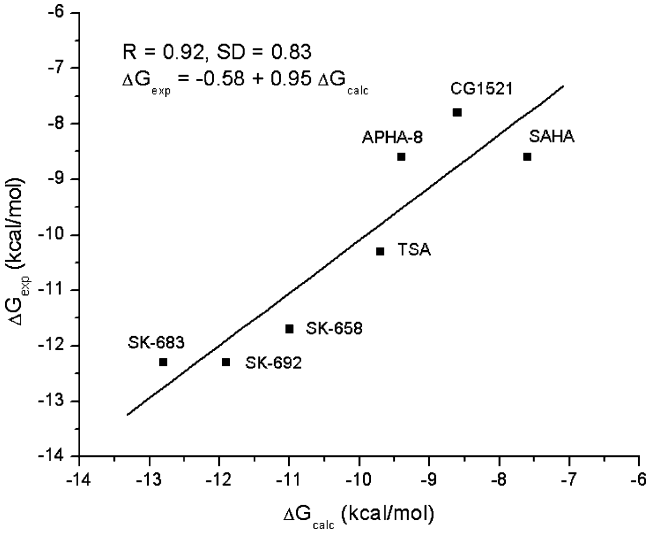

Figure 6. Linear regression of estimated free energy of binding from AutoDock vs experimental values derived from IC_{50}.

Estimated Free Energies of Binding. The estimated free energy of binding of the best docked structure of TSA is −9.7kcal/mol. The best value obtained for SAHA is −7.6 kcal/mol. These results agree with the experimental observation of stronger binding of TSA than SAHA to HDAC. More interestingly, all the calculated free energies of binding of TSA, SAHA, SK-658, SK-683, SK-692, and CG1521 are close to the values derived from the experimental IC_{50} values.[7] In fact, our results demonstrate a reasonably good linear relationship between estimated free energy of binding from docking and experimental inhibition activity as shown in Figure 6. Part of the reason for this good relationship is the estimation of free energy function of AutoDock which is derived from a large database of diverse protein−ligand complexes with known inhibition constants through a linear regression-like QSAR technique for estimation of inhibition constants. Good agreement has been reported between estimated free energies of binding and experimental values for HIV integrase−ligand systems.[14] The correlation coefficient of $R = 0.92$ seen in the present study is much better than commonly expected for the relatively simple scoring function of AutoDock and should not be generalized. Nevertheless, it appears that the correlation is excellent at least for this system and thus increases our confidence that the activity of new HDAC inhibitors can be estimated fairly accurately using AutoDock.

Function of 14 Å Internal Cavity of HDLP or HDAC1. With these promising results in hand, we now return to the previously found novel binding mode of CG1521. Although the shape of the entrance channel makes the alternative binding mode shown in Figure 4 unlikely, it does hint at the possible role of the internal cavity, which is presently not well understood. To investigate other possibilities for interactions at the Zn binding site and the cavity, we performed AutoDock calculations with three different small probe molecules: *N*-hydroxyacetamide to explore the competition between metal binding and polar interactions, and acetate and acetic acid as models for the interaction of the protonated and deprotonated hydrolysis product with the hydrolytic center. Analysis of these results should give insight into the role of the cavity and a better understanding of the hydrolytic process.

The results of the acetate and the acetic acid docking calculations are summarized in Figure 7A and 7B. For acetic acid, the structures in the two strongest binding clusters with free energies of binding of −4.0 and −3.8 kcal/mol, respectively, are found near the hydrolytic center, named Region I. There is a second cluster of binding sites for acetic acid in Region III, where it interacts with the Arg16 residue, with a ΔG_{cal} of −3.7 kcal/mol.[30] Finally, hydrogen bonding interactions with Arg27 leads to binding of acetic acid in a region between Regions I and III, named Region II in Figure 7A. Interestingly, none of the favorable binding sites are located in the 11 Å channel. Region III is the bottom of the internal 14 Å cavity, while Region I is at the connection between the 11 Å channel and the internal cavity. It may therefore be deduced that the function of the internal cavity is to accommodate the hydrolysis product, acetic acid or acetate. Comparison of the free energies of binding from the AutoDock calculations shows that the binding abilities of acetic acid in the three regions are quite similar.

Docking of acetate into the active site further supports the above results.[31] As expected, acetate has stronger Zn binding ability than acetic acid due to acetate's anionic character. Structures in the eleven strongest binding clusters are located at the hydrolytic center, Region I (green-colored structures in Figure 7B). Their binding free energies range from −5.3 to −5.0 kcal/mol. Cluster 12 (orange-colored structure in Figure 7B belonging to Region III) contains 26 out of a total of 100 structures and has a binding free energy of −3.8 kcal/mol. In Region II, acetate (cyan-colored structure in

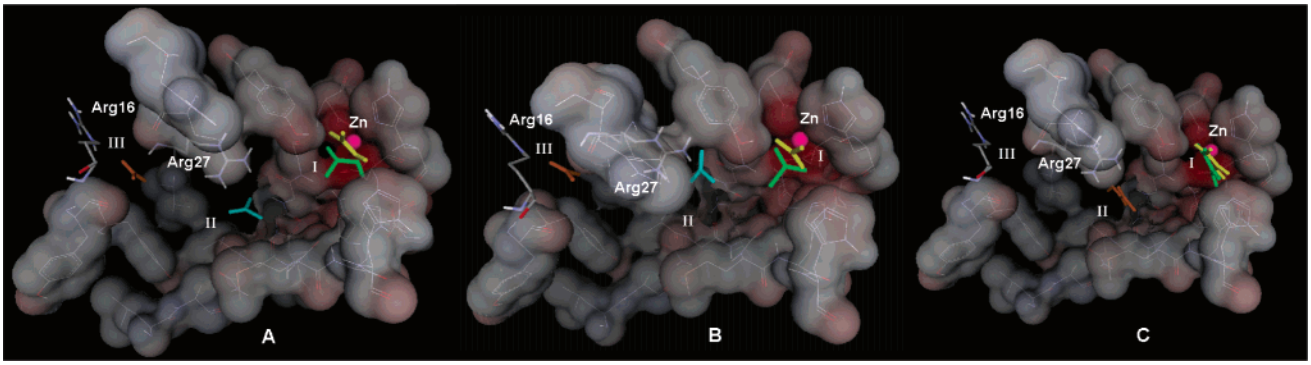

Figure 7. Calculated binding modes (Region I, II, and III) of acetic acid (A), acetate (B), and *N*-hydroxyacetamide (C) in the 14 Å internal cavity of HDLP.

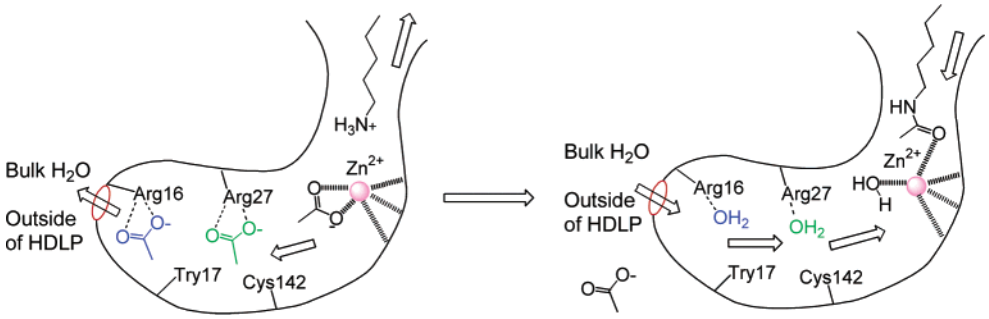

Figure 8. Picture of internal cavity after deacetylation. While the free lysine chain is leaving the 11 Å channel, the byproduct acetate is passing through the 14 Å cavity. The catalytic center therefore is ready to accept the water and acetylated lysine for the next cycle of hydrolysis.

Figure 7B) was also found with a binding free energy of −2.6 kcal/mol. Again, no low-energy binding sites were found in the 11 Å channel. Although the binding of acetate is slightly more exothermic than that of acetic acid, the difference in the desolvation penalty between neutral acetic acid and anionic acetate needs to be considered. Therefore, compared to the alternative binding sites in Regions II and III, it is expected that acetate will not bind strongly to the Zn binding site. It is well-known that acetic acid and acetates are not good zinc binders.[32] The importance of the anionic character of the acetate for binding in the internal cavity is demonstrated by docking of *N*-hydroxyacetamide, a simple model of the binding motif of known inhibitors TSA, SAHA, and CG1521. Again, the strong binding sites were found in Region I and Region II. The lowest free energy of binding of −5.6 kcal/mol was calculated for the green-colored structure in Figure 7C.

These results raise a number of questions for the steps before and after the actual hydrolysis that have implications for the design of new HDAC inhibitors. First, how does the byproduct of the hydrolysis, the acetate, leave the active site if the docking calculations predict there is not favorable interactions for acetate along the exit channel used by the lysine chain? Second, how is the water necessary for hydrolysis transported into the active site, which is buried deeply along the narrow, hydrophobic 11 Å channel? Consideration of these questions led us to a new hypothesis for the role of the internal cavity for the function of HDLP or HDAC1. We postulate that after the hydrolytic reaction, while the protonated lysine side chain is leaving the catalytic center via the 11 Å channel, the acetate or acetic acid could remain in the 14 Å internal cavity since there are no favorable binding sites along the 11 Å channel and the channel is still occupied by the protonated lysine side chain. The L1 loop (Lys14-Arg27), which separates the 14 Å internal cavity from the solvent exposed surface of the enzyme, has considerable mobility as judged by its larger temperature factor (B-factor) than the rest of the structure.[10] For example, Arg16, which is located at the very end of the internal cavity, has a B-factor of 67.0 $Å^2$ in the X-ray structure. This indicates that the cavity contents may exchange with the bulk solvent. Therefore, the possibility arises that the acetate does not leave via the channel, but rather passes through the 14 Å cavity as shown in Figure 8. The first binding site for the acetic acid or acetate could be Arg27 which then is in equilibrium with Arg16, another binding site at the bottom of the cavity. Side chain

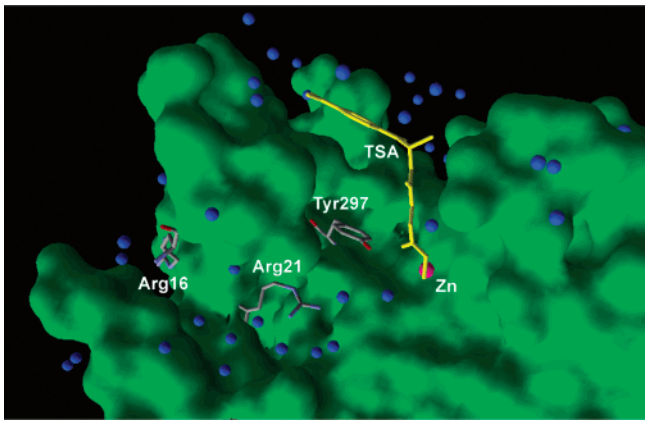

Figure 9. Water distribution in the internal cavity and surface of HDLP. Blue dots represent water molecules. Picture directly generated from chain A of X-ray structure 1c3r.[10]

movement of the surface-exposed Arg16 could then bring the acetic acid or acetate out of the 14 Å cavity and exchange it with the bulk water. Conversely, the uptake of water molecules in the opposite direction could regenerate the activity of the hydrolytic center. If the acetate could not leave the hydrolytic center rapidly, it would block the center and hinder the substrate binding. In the X-ray structure, a number of waters are found in the 14 Å internal cavity as shown in Figure 9, although the cavity is considered to be hydrophobic and only a few polar residues, such as Arg27 and His21, are located there. One could argue that acetate could diffuse faster from the 11 Å channel due to the absence of a favorable binding site there. However, after the hydrolytic reaction, the 11 Å channel is occupied by the lysine long chain. This suggests that both the lysine chain and the acetate leave the hydrolytic center simultaneously in different directions instead of separately from the same channel. Although our result is based on the HDLP structure, the sequence and structural similarity of HDLP and HDAC in the 14 Å cavity suggests it has the same function in both proteins.

The significance of our results is that they suggest a novel concept to direct further HDAC inhibitor design. While the principal functional group of the ligand binds to the Zn center, an additional side chain of the ligand may be designed to bind into the 14 Å long cavity. This site provides an alternative to binding in the 11 Å straight channel or at the entrance to this channel, on which most of the previous design work has focused. Figure 10 shows the proposed new strategy for HDAC inhibitor design. Here, a second binding element de-

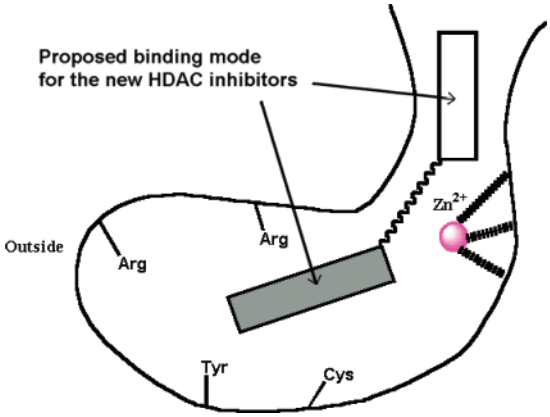

Figure 10. Proposed new strategy for HDAC inhibitor design.

signed to occupy the 14 Å long cavity is attached to the zinc binding unit, for example via covalent attachment to the metal chelator group. Based on this hypothesis, further inhibitor design and synthesis are underway in our laboratory.

In summary, we have shown that the AutoDock scoring function can be adapted successfully to metalloenzymes such as HDAC. The structures and free energy of binding thus obtained are in good agreement with the available experimental data for a wide range of hydroxamic acid-based HDAC inhibitors. It can therefore be expected that the method provides a fast and reliable tool for the investigation of new HDAC inhibitors. Examples of applications include a series of new HDAC inhibitors incorporating a tribenzyl unit that are currently being studied in our laboratories as well as the use of probe molecules to explore binding interactions in the active site of HDAC. Results from the latter calculations led us to hypothesize that the function of the 14 Å internal cavity is to accommodate the byproduct, acetate or acetic acid, of the hydrolytic reaction. This finding could significantly benefit the future design of HDAC inhibitors.

Acknowledgment. The authors thank Prof. Marvin J. Miller and Dr. Jayne Oliver for valuable discussions. Additional support for computational resources from the National Science Foundation (DMR0079647) and collaboration with the Walther Cancer Institute is also gratefully acknowledged.

Supporting Information Available: Detailed information about building the homology model of human HDAC1, Procheck results (Figure 16), the surface representation of the channel and the internal cavity of human HDAC1 model (Figure 12), and Figures 11, 13−15 are available free of charge via the Internet at http://pubs.acs.org. Coordinates (pdb format) of all structures are available from the authors upon request.

References

(1) Pazin, M. J.; Kadonaga, J. T. What is up and down with histone deacetylation and transcription? *Cell* **1997**, *89*, 325−328. (b) Pennisi, E. Opening the way to gene activity. *Science* **1997**, *275*, 155−157.

(2) Yoshida, M.; Kijima, M.; Akita, M.; Beppu, T. Potent and specific inhibition of mammalian histone deacetylases both in vivo and in vitro by trichostatin A. *J. Biol. Chem.* **1990**, *265*, 17174−17179.

(3) Richon, V. M.; Emiliani, S.; Verdin, E.; Webb, Y.; Breslow, R.; Rifkind, R. A.; Marks, P. A. A class of hybrid polar inducers of transformed cell differentiation inhibits histone deacetylases. *Proc. Natl. Acad. Sci. U.S.A.* **1998**, *95*, 3003−3007.

(4) Han, J. W.; Ahn, S. H.; Park, S. H.; Wang, S. Y.; Bae, G. U.; Seo, D. W.; Known, H. K.; Hong, S.; Lee, Y. W.; Lee, H. W. Apicidin, a histone deacetylase inhibitor, inhibits proliferation of tumor cells via induction of p21WAF1/Cip1 and gelsolin. *Cancer Res.* **2000**, *60*, 6068−6074.

(5) Kijima, M.; Yoshida, M.; Suguta, K.; Horinouchi, S.; Beppu, T. Trapoxin, an antitumor cyclic tetrapeptide, Is an irreversible inhibitor of mammalian histone deacetylases. *J. Biol. Chem.* **1993**, *268*, 22429−22435.

(6) (a)Jung, M.; Brosh, G.; Kölle, D.; Schef, H.; Gerhöuser, C.; Loidl, P. Amide analogues of trichostatin A as inhibitors of histone deacetylase and inducers of terminal cell differentiation. *J. Med. Chem.* **1999**, *42*, 4669−4679. (b) Jung, M.; Hoffmann, K.; Brosch, G.; Loidl, P. Analogues of Trichostatin A and Trapoxin B as histone deacetylase inhibitors. *Bioorg. Med. Chem. Lett.* **1997**, *7*, 1655−1658. (c) Suzuki, T.; Ando, T.; Tsuchiya, K.; Fukazawa, N.; Saito, A.; Mariko, Y.; Yamashita, T.; Nakanishi, O. Synthesis and histone deacetylase inhibitory activity of new benzamide derivatives. *J. Med. Chem.* **1999**, *42*, 3001−3003. (d) Furumai, R.; Komatsu, Y.; Nishino, N.; Khochbin, S.; Yoshida, M.; Horinouchi, S. Potent histone deacetylase inhibitors built from trihostatin A and cyclic tetrapeptide antibiotics including trapoxin. *Proc. Natl. Acad. Sci. U.S.A.* **2001**, *98*, 87−92. (e) Massa, S.; Mai, A.; Sbardella, G.; Esposito, M.; Ragno, R.; Loidl, P.; Brosch, G. 3-(4-Aroyl-1*H*-prrol-2-yl)-*N*-hydroxy-2-propenamides, a new class of synthetic histone deacetylase inhibitors. *J. Med. Chem.* **2001**, *44*, 2069−2072. (f) Lavoie, R.; Bouchain, G.; Frechette, S.; Woo, S. H.; Khalil, E. A.; Leit, S.; Fournel, M.; Yan, P. T.; Trachy-Bourget, M.-C.; Beaulieu, C.; Li, Z.; Besterman, J.; Jelorme, D. Design and synthesis of a novel class of histone deacetylase inhibitors. *Bioorg. Med. Chem. Lett.* **2001**, *11*, 2847−2850.

(7) (a) Wang, D.-F.; Wiest, O. G.; Helquist, P. Lan-Hargest, H.-Y.; Wiech, N. L. QSAR studies of PC-3 cell line inhibition activity of TSA and SAHA-like hydroxamic acids. *Bioorg. Med. Chem. Lett.* **2004**, *14*, 707−711. (b) Lan-Hargest, H.-Y.; Kaufman, R. J.; Wiech, N. L. US Patent Appl. US20020143196.

(8) (a) Cohen, L. A.; Amin, S.; Marks, P. A.; Rifkind, R. A.; Desai, D.; Richon, V. M. Chemoprevention of carcinogen-induced mammary tumorigenesis by the Hybrid Polar Cytodifferentiation agent, suberanilohydroxamic acid (SAHA) *Anticancer Res.* **1999**, *19*, 4999−5005. (b) Desai, D., El-Nayoumy, K.; Amin, S. Chemopreventive efficacy of suberanilohydroxamic acid (SAHA), a cytodifferentiating agent, against tobacco-specfic nitrosamine 4-(methylinitros-amino)-1-(3-pyridyl)-1-butanone (NNK)-induced lung tumorigenesis in female A/J mice. *Proc. Am. Assoc. Cancer Res.* **1999**, *40*, 2396, abstr. 362.

(9) (a) Miller, T. A.; Witter, D. J.; and Belvedere, S. Histone deacetylase inhibitors *J. Med. Chem.* **2003**, *46*, 5096−5115 and reference therein. (b) Yoshida, M.; Matsuyama, A.; Komatsu, Y.; Nishino, N. From discovery to the coming generation of histone deacetylase inhibitors. *Curr. Med. Chem.* **2003**, *10*, 2351−2358.

(10) Finnin, M. S.; Donigian, J. R.; Cohen, A.; Richon, V. M.; Rifkind, R. A.; Marks, P. A.; Breslow, R.; Pavletich, N. P. Structures of a Histone Deacetylase Homologue Bound to the TSA and SAHA Inhibitors. *Nature* **1999**, *401*, 188−193.

(11) Homology model of HDAC1 was built with Modeller4 program [Sali, A.; Blundell, T. L. Comparative protein modeling by satisfaction of spatial restraints. *J. Mol. Biol.* **1993**, *234*, 779−815. http://salilab.org/modeller/modeller.html]. The model was minimized by Amber6 program with 2000 steps. It was further checked by PROCHECK program [(a) Laskowski, R. A.; MacArthur, M. W.; Moss, D. S. and Thornton, J. M. PROCHECK: a program to check the stereochemical quality of protein structures. *J. Appl. Crystallogr.* **1993**, *26*, 283−291. (b) Morris, A. L.; MacArthur, M. W.; Hutchinson, E. G. and Thornton, J. M. Stereochemical quality of protein structure coordinates. *Proteins* **1992**, *12*, 345−364. http://www.biochem.ucl.ac.uk/~roman/procheck/procheck.html.]

(12) Gregoretti, I.; Lee, Y.-M.; Goodson, H. V. Molecular Evolution of the Histone Deacetylase Family: Functional Implications of Phylogenetic Analysis. *J. Mol. Biol.* **2004**, *338*, 17−31.

(13) Morris, G. M.; Goodsell, D. S., Halliday, R. S., Huey, R., Hart, W. E., Belew, R. K.; Olson, A. J. Automated Docking Using a Lamarckian Genetic Algorithm and Empirical Binding Free Energy Function. *J. Comput. Chem.* **1998**, *19*, 1639−1662. http://www.scripps.edu/pub/olson-web/doc/autodock/.

(14) (a) Perryman, A.; McCammon, J. A. Autodocking Dinucleotides to the HIV-1 Integrase Core Domain: Exploring Possible Binding Sites For Viral and Genomic DNA. *J. Med. Chem.* **2002**, *45*, 5624−5627. (b) Sotriffer, C. A., Ni, H.; McCammon, J. A. Active Site Binding Modes of HIV-1 Integrase Inhibitors. *J. Med. Chem.* **2000**, *43*, 4109−4117. (c) Sotriffer, C. A., Ni, H.; McCammon HIV-1 Integrase Inhibitors Interactions at the Active Site: Prediction of Binding Modes Unaffected by Crystal Packing. *J. Am. Chem. Soc.* **2000**, *122*, 6136−6137.

(15) AutoDockTools can be downloaded free of charge from this website: http://www. scripps.edu/pub/olson-web/doc/autodock/tools.html.

(16) In 1c3r, there are two HDLP−TSA complexes. Only the A-form structure was considered in our study.
(17) Berman, H. M.; Westbrook, J.; Feng, Z.; Gilliland, G.; Bhat, T. N.; Weissig, H.; I. N. Shindyalov, I. N.; Bourne, P. E. The Protein Data Bank. *Nucleic Acids Res.* **2000**, *28*, 235−242. Website: http://www.rcsb.org/pdb/.
(18) Case, D. A.; Pearlman, D. A.; Caldwell, J. W.; Cheatham, T. E., III; Ross, W. S.; Simmerling, C. L.; Darden, T. A.; Merz, K. M.; Stanton, R. V.; Cheng, A. L.; Vincent, J. J.; Crowley, M.; Tsui, V.; Radmer, R. J.; Duan, Y.; Pitera, J.; Massova, I.; Seibel, G. L.; Singh, U. C.; Weiner, P. K.; Kollman, P. A. Amber6.0, University of California, San Francisco CA, 1999. http://amber-.scripps.edu/.
(19) Gaussian 98, A.9, Frisch, M. J.; Trucks, G. W.; Schlegel, H. B.; Scuseria, G. E.; Robb, M. A.; Cheeseman, J. R.; Zakrzewski, V. G.; Montgomery, J. A., Jr.; Stratmann, R. E.; Burant, J. C.; Dapprich, S.; Millam, J. M.; Daniels, A. D.; Kudin, K. N.; Strain, M. C.; Farkas, O.; Tomasi, J.; Barone, V.; Cossi, M.; Cammi, R.; Mennucci, B.; Pomelli, C.; Adamo, C.; Clifford, S.; Ochterski, J.; Petersson, G. A.; Ayala, P. Y.; Cui, Q.; Morokuma, K.; Malick, D. K.; Rabuck, A. D.; Raghavachari, K.; Foresman, J. B.; Cioslowski, J.; Ortiz, J. V.; Stefanov, B. B.; Liu, G.; Liashenko, A.; Piskorz, P.; Komaromi, I.; Gomperts, R.; Martin, R. L.; Fox, D. J.; Keith, T.; Al-Laham, M. A.; Peng, C. Y.; Nanayakkara, A.; Gonzalez, C.; Challacombe, M.; Gill, P. M. W.; Johnson, B. G.; Chen, W.; Wong, M. W.; Andres, J. L.; Head-Gordon, M.; Replogle, E. S.; Pople, J. A. Gaussian, Inc.: Pittsburgh, PA, 1998. http://www.Gaussian.com/.
(20) (a)Rao, M. S.; Olson, A. J. Modelling of factor Xa-inhibitor complexes: a computational flexible docking approach. *Proteins* **1999**, *34*, 173−83. (b)Tummino, P. J., Ferguson, D., Jacobs, C. M.; Tait, B.; Hupe, L.; Lunney, E.; Hupe, D. Competitive inhibition of HIV-1 protease by biphenyl carboxylic acids. *Arch. Biochem. Biophys.***1995**, *316*, 523−528.
(21) (a)Sotriffer, C. A.; Flader, W.; Winger, R. H.; Rode, B. M.; Liedl, K. R.; Varga, J. M. Automated docking of ligands to antibodies: methods and applications. *Methods* **2000**, *20*, 280−291. (b)-Stoddard, B. L.; Koshland, D. E., Jr. Prediction of a receptor protein complex using a binary docking method. *Nature* **1992**, 358, 774−776.
(22) (a) Minke, W. E., Diller, D. J., Hol, W. G., Verlinde C. L. The role of waters in docking strategies with incremental flexibility for carbohydrate derivatives: heat-labile enterotoxin, a multivalent test case. *J. Med. Chem.* **1999**, *42*, 1778−1788. (b) Laederach, A.; Dowd, M. K.; Coutinho, P. M.; Reilly, P. J. Automated Docking of Maltose, 2-Deoxymaltose, and Maltotetraose into the Soybean beta-Amylase Active Site. *Protein* **1999**, *37*, 166−175. (c) Bitomsky, W.; Wade, R. C. Docking of Glycosaminoglycans to Heparin-Binding Proteins: Validation foraF-GF, bFGF, and Antithrombin and Application to IL-8. *J. Am. Chem. Soc.* **1999**, *121*, 3004−3013.
(23) (a) Chang, Y. T.; Veitch, N. C.; Loew G. H. A Theoretical Study of Benzhydroxamic Acid Binding Modes in Horseradish Peroxidase. *J. Am. Chem. Soc.* **1998**, *120*, 5168−5178. Compare also: (b) Perola, E.; Xu, K.; Kollmeyer, T. M.; Kaufmann, S. H.; Prendergast, F. G.; Pang, Y.-P. Successful Virtual Screening of a Chemical Database for Farnesyltransferase Inhibitor Leads. *J. Med. Chem.* **2000**, *43*, 401−408.
(24) (a) Stote, R. H.; Karplus, M. Zinc-binding in proteins and solution- a simple but accurate nonbonded representation. *Proteins* **1995**, *23*, 12−31. For an alternative parametrization, see: (b) Hu, X.; Shelver, W. H. Docking studies of matrix metalloproteinase inhibitors: zinc parameter optimization to improve the binding free energy prediction *J. Mol. Graph. Mod.* **2003**, *22*, 115−126.
(25) (a) Donini, O. A. T.; Kollman, P. A. Calculation and prediction of binding free energies for the matrix metalloproteinases. *J. Med. Chem.* **2000**, *43*, 4180−4188. (b) Terp, G. E.; Christensen, I. T.; Jorgensen, F. S. Structural differences of matrix metalloproteinases. Homology modeling and energy minimization of enzyme−substrate complexes. *J. Biomol. Struct. Dyn.* **2000**, *17*, 933−946.
(26) Raha, K.; Merz, K. M., Jr. A Quantum Mechanics-Based Scoring Function: Study of Zinc Ion-Mediated Ligand Binding. *J. Am. Chem. Soc.* **2004**, *126*, 1020−1021.
(27) Richon, V. M.; Marks, P. A.; Rifkind, R. A.; Breslow, R.; Belvedere, S. International. Patent WO 01/18171 A2, 2001.
(28) (a) Mai, A.; Massa, S.; Ragno, R.; Cerbara, I.; Jesacher, F.; Loidl, P.; Brosch G. 3-(4-Aroyl-1-methyl-1*H*-2-pyrrolyl)-*N*-hydroxy-2-alkylamides as a New Class of Synthetic Histone Deacetylase Inhibitors. 1. Design, Synthesis, Biological Evaluation, and Binding Mode Studies Performed through Three Different Docking Procedures. *J. Med. Chem.* **2003**, *46*, 512−524. (b) Mai, A.; Massa, S.; Ragno, R.; Esposito, M.; Sbardella, G.; Nocca, G.; Scatena, R.; Jesacher, F.; Loidl, P.; Brosch, G. Binding Model Analysis of 3-(4-Benzoyl-1-methyl-1-H-2-pyrrolyl)-N-hydroxy-2-propenamide: A New Synthetic Histone Deacetylase Inhibitor Inducing Histone Hyperacetylation, Grouth Inhibition, and Terminal Cell Differentiation. *J. Med. Chem.* **2002**, *45*, 1778−1784.
(29) Löfstedt, J.; Chaverri, J.; Wang, D.-F.; Goodson, H.; Wiest, O.; Helquist, P. Unpublished results.
(30) The structures in this region belong to clusters 4 and 5. The structure in cluster 3 is not in region II or I.
(31) In this case, the HDLP structure was modified by changing His131 from its neutral form to its protonated form in order to balance the amount of hydrogen atoms before and after the hydrolytic reaction.
(32) Martin, R. B. *Metal Ions in Biological Systems*; Sigel, H., Ed.; Marcel Dekker: New York, 1986; Vol. 20, p 21.

JM0498497